

Measurements of Attenuation and Absorption Lengths with the KASCADE Experiment

T. Antoni ^a, W. D. Apel ^b, A.F. Badea ^{a,1}, K. Bekk ^b, A. Bercuci ^{b,1},
 H. Blümer ^{b,a}, H. Bozdog ^b, I. M. Brancus ^c, C. Büttner ^a,
 A. Chilingarian ^d, K. Daumiller ^a, P. Doll ^b, R. Engel ^b, J. Engler ^b,
 F. Feßler ^b, H. J. Gils ^b, R. Glasstetter ^a, R. Haeusler ^a, A. Haungs ^b,
 D. Heck ^b, J. R. Hörandel ^a, A. Iwan ^{a,2}, K.-H. Kampert ^{a,b},
 H. O. Klages ^b, G. Maier ^{b,3}, H. J. Mathes ^b, H. J. Mayer ^b, J. Milke ^b,
 M. Müller ^b, R. Obenland ^b, J. Oehlschläger ^b, S. Ostapchenko ^{a,4},
 M. Petcu ^c, H. Rebel ^b, M. Risse ^b, M. Roth ^b, G. Schatz ^b,
 H. Schieler ^b, J. Scholz ^b, T. Thouw ^b, H. Ulrich ^b, A. Vardanyan ^d,
 J. H. Weber ^a, A. Weindl ^b, J. Wentz ^b, J. Wochele ^b, J. Zabierowski ^e

(The KASCADE Collaboration)

^a*Institut für Experimentelle Kernphysik, University of Karlsruhe, 76021 Karlsruhe, Germany*

^b*Institut für Kernphysik, Forschungszentrum Karlsruhe, 76021 Karlsruhe, Germany*

^c*National Institute of Physics and Nuclear Engineering, 7690 Bucharest, Romania*

^d*Cosmic Ray Division, Yerevan Physics Institute, Yerevan 36, Armenia*

^e*Soltan Institute for Nuclear Studies, 90950 Lodz, Poland*

¹ on leave of absence from NIPNE, Bucharest

² and University of Lodz, Lodz, Poland

³ corresponding author, email: gernot.maier@ik.fzk.de

⁴ on leave of absence from Moscow State University, Moscow, Russia

Abstract

The attenuation of the electron shower size beyond the shower maximum is studied with the KASCADE extensive air shower experiment in the primary energy range of about $10^{14} - 10^{16}$ eV. Attenuation and absorption lengths are determined by applying different approaches, including the method of constant intensity, the decrease of the flux of extensive air showers with increasing zenith angle, and its variation with ground pressure. We observe a significant dependence of the results on the applied method. The determined values of the attenuation length ranges from 175 to 196 g/cm^2 and of the absorption length from 100 to 120 g/cm^2 . The origin of these differences is discussed emphasizing the influence of intrinsic shower fluctuations.

Key words: cosmic rays; extensive air showers; attenuation length

PACS: 96.40.Pq

1 Introduction

The longitudinal development of the electron shower size N_e in extensive air showers (EAS) is characterized by an approximately exponential decline for atmospheric depths well beyond the shower maximum. Therefore, N_e shows a strong dependence on the slant depth. The magnitude of this effect is usually described by two different quantities, the attenuation and the absorption length.

In the following the attenuation length Λ_{N_e} describes the average decrease of the electron number N_e with increasing atmospheric depth X in showers selected to be similar in primary energy:

$$\langle N_e(X) \rangle \propto \exp(-X/\Lambda_{N_e}) \quad (1)$$

The absorption length Λ_{rate} is defined to parameterize the decrease of the integral flux $j(> N_e)$ of showers with electron numbers greater than N_e at a given atmospheric depth X :

$$j(> N_e, X) \propto \exp(-X/\Lambda_{rate}) \quad (2)$$

Both quantities are frequently used to rescale showers to a certain angle of incidence [1,2], i.e. atmospheric depth, or for applying ground pressure corrections.

There exist various different methods to determine the attenuation respectively the absorption length. The purpose of this paper is to determine Λ_{N_e} and Λ_{rate} from one set of experimental data by applying different methods. The results are then

compared to each other in order to estimate systematic uncertainties resulting from the different approaches.

It should be emphasized that there is a conceptual difference between the attenuation and the absorption length. The absorption length Λ_{rate} depends on the form and steepness of the primary energy spectrum and is only defined for a set of showers while the definition of the attenuation length Λ_{N_e} is independent of that and applicable to individual showers. However, the methods used in this analysis do not allow to measure the attenuation length Λ_{N_e} on a shower-by-shower basis. Therefore only an effective Λ_{N_e} is measured which describes the shape of a mean shower at atmospheric depths much larger than the depth of the shower maximum.

Assuming a pure composition and a power law of the electron shower size spectrum, the relation between attenuation and absorption length reads $\Lambda_{N_e} = (\gamma - 1) \cdot \Lambda_{rate}$, with the spectral index γ . For a mixed composition or other spectral shapes, the relation is much more complicated. A further difficulty in these relations are shower fluctuations which depend on shower size and angle and modify the shower size spectra.

The definition of the absorption length Λ_{rate} in Equation (2) is different from the one frequently used to infer proton-air cross section from EAS with the constant N_e - N_μ -Method (e.g. [3] and Chapter 6). In the following, absorption of showers without any preselection by the muon shower size is analyzed.

The paper is organized in the following way. Chapter 2 describes the experimental setup and the reconstruction of EAS with the KASCADE experiment. Two different methods to determine the attenuation length are presented in Chapter 3. Both are based on a selection of showers above approximately the same primary energy. This is done by considering the shift of the knee position with increasing zenith angle or by applying constant intensity cuts to spectra in different angular bins. Chapter 4 describes the analysis of the spectra with regard to the absorption length by examining the variation of the rate with angle of incidence or atmospheric ground pressure. Since all quantities related to EAS, especially the electron shower size, are influenced by intrinsic shower fluctuations, we estimate the magnitude of these effects in Chapter 5. A short remark about the already mentioned constant N_e - N_μ -Method is given in Chapter 6 and a summary is given in Chapter 7.

2 KASCADE - experimental setup and EAS reconstruction

KASCADE (*KArlsruhe Shower Core and Array DEtector*) [4,5] is located at Forschungszentrum Karlsruhe, Germany (8.4° E, 49.1° N) at 110 m a.s.l. corresponding to an average vertical atmospheric depth of 1022 g/cm². The experiment measures the electromagnetic, muonic, and hadronic components of EAS with three major

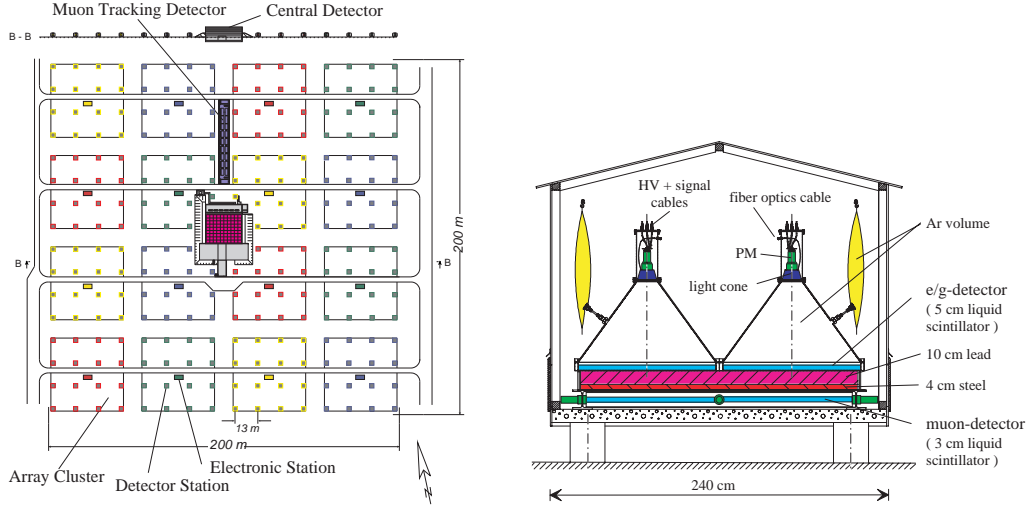


Fig. 1. Schematic view of the KASCADE field array and a detector station

detector systems, a large field array, a muon tracking detector, and a central detector.

In the present analysis data from the $200 \times 200 \text{ m}^2$ scintillation detector array shown in Figure 1 are used. The 252 detector stations of the array are uniformly spaced on a grid with a separation of 13 m. The stations are organized in 16 electronically independent clusters with 16 stations in the 12 outer and 15 stations in the four inner clusters. The array stations contain four detectors measuring the electromagnetic component in the four inner resp. two in the 12 outer clusters. They are filled with 5 cm thick custom made liquid scintillator with an area of 0.8 m^2 each. The 192 stations in the 12 outer clusters are additionally equipped with four sheets of plastic scintillation detectors, $90 \times 90 \times 3 \text{ cm}^3$ each. These detectors, mounted below 10 cm absorber of lead and 4 cm of iron, which corresponds to more than 20 radiation lengths and to a muon energy threshold of 230 MeV, are used to measure the muonic component of an air shower. The energy sum, the arrival time of the first shower particle in a station, and the hit pattern of the detectors are read out individually for the muon and e/γ detectors. The trigger conditions are a detector multiplicity of 10/20 out of 32/60 e/γ detectors fired in at least one of the outer/inner clusters.

The scintillator array reaches full trigger and reconstruction efficiency for showers with $\log_{10} \bar{N}_e > 4.3$ almost independent of the type of the primary particle. In the following analysis, only showers safely above this threshold are used.

In an iterative shower reconstruction procedure the electron shower size and slope of the lateral electron distribution ('age') are determined mainly by maximizing a likelihood function describing the measurements with the Nishimura Kamata Greisen (NKG) formula [6,7] assuming a Molière radius of 89 m. Detector signals are corrected for contributions of other particles, i.e. the electromagnetic detectors

for contributions of muons, gammas, and hadrons. A detailed presentation of these corrections can be found in [8].

Shower cores are identified in a first step by the center of gravity of the energy deposits in the detectors and in a second iteration by the NKG-fit mentioned above. Shower directions are determined by fitting a conical shower front to the measured particle arrival times.

For the present analysis showers have been selected with reconstructed shower cores inside a circle of 91 m around the center of the array and with zenith angles less than 40° . This results in a set of about 37 million well reconstructed showers.

The influence of the sampling fluctuation on the results of the following analysis is examined in Chapter 5. Detailed descriptions of the detectors and reconstruction performances are given in [4,5].

3 Attenuation length Λ_{N_e}

The idea of the following analysis is to select showers of a certain primary energies and then to observe the attenuation of their electron shower size N_e with increasing atmospheric depth. Assuming a functional dependence between the primary energy spectra and the electron shower size spectra, application of equal intensity cuts to the integral electron shower size spectra in different angular bins select showers above approximately equal primary energies. This is the method of constant intensity [9].

Assuming the knee to be of astrophysical origin, i.e. to be a feature of the primary energy spectrum, the method of constant intensity can be applied in a special way to determine the attenuation of the shower size at the knee. One has to keep in mind, however, that the shapes of electron shower size spectra are influenced by intrinsic shower fluctuations which in turn show variations with electron shower size and incident angle of the EAS. Therefore, the knee positions in the electron shower size spectra is shifted in a non-trivial way and differently in the various bins of zenith angle towards larger shower sizes.

Attenuation is observed in the following by analyzing showers in different angular bins. Equation (1) then becomes:

$$\langle N_e(\Theta) \rangle \propto \exp\left(-\frac{X_0}{\Lambda_{N_e}}(\sec \Theta - 1)\right). \quad (3)$$

$X_0 = 1022 \text{ g/cm}^2$ is the average vertical atmospheric depth at the KASCADE observation level and Θ is the zenith angle of the EAS.

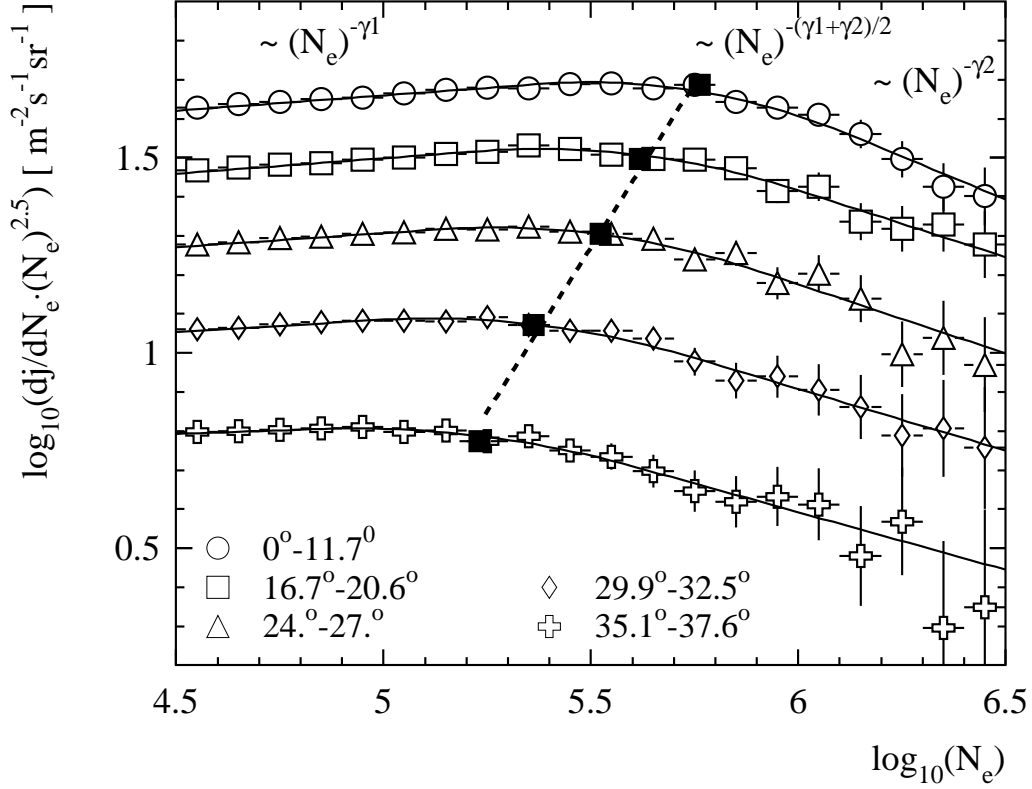


Fig. 2. Differential electron shower size spectra measured by the KASCADE experiment. The shift of the knee position with increasing zenith angle is indicated by the dotted line. The solid lines indicate the fits described in the text. Only size spectra of every second angular bin are plotted.

3.1 Position of the knee

Figure 2 shows the differential electron shower size spectra in the knee region as measured with the KASCADE experiment for different angular bins. The shift of the knee position with increasing atmospheric depth is clearly visible.

Spectra in 10 different angular bins ranging from 0° to 40° were analyzed. The angular bins are selected to cover the same solid angle. For reasons of clarity, only every second spectrum is plotted in Figure 2. The spectra are fitted with the following function [10]:

$$dj/dN_e \propto \begin{cases} N_e^{-\gamma_1} & \log_{10} N_e \leq \log_{10} N_{e,k} - \epsilon \\ N_e^{a_2 \log_{10} N_e + a_1} & \log_{10} N_{e,k} - \epsilon < \log_{10} N_e < \log_{10} N_{e,k} + \epsilon \\ N_e^{-\gamma_2} & \log_{10} N_e \geq \log_{10} N_{e,k} + \epsilon \end{cases} \quad (4)$$

with the electron shower size at the knee $N_{e,k}$. Fit parameters are the two spectral

Table 1
Results of the fits of Equation (4) to the electron size spectra.

angular bin	position of the knee $\log_{10}(N_e)$	integral flux above the knee $[10^{-8} \text{ m}^{-2} \text{ s}^{-1} \text{ sr}^{-1}]$
0.0° – 11.7°	5.76 ± 0.03	6.47 ± 0.35
11.7° – 16.7°	5.65 ± 0.03	8.43 ± 0.40
16.7° – 20.6°	5.62 ± 0.03	7.58 ± 0.36
20.6° – 24.0°	5.59 ± 0.03	6.73 ± 0.38
24.0° – 27.0°	5.52 ± 0.03	6.57 ± 0.43
27.0° – 29.9°	5.46 ± 0.04	6.49 ± 0.48
29.9° – 32.5°	5.36 ± 0.04	6.80 ± 0.49
32.5° – 35.1°	5.33 ± 0.04	5.41 ± 0.44
35.1° – 37.6°	5.23 ± 0.05	5.56 ± 0.45
37.6° – 40.0°	5.07 ± 0.06	6.70 ± 0.64

indices, γ_1 , γ_2 , the size at the knee, $\log_{10} N_{e,k}$, the half width ϵ , and the differential flux at the knee. The half width ϵ of the knee region is constant within the statistical errors and therefore fixed to $\epsilon = 0.38$ on a logarithmic shower size scale in these fits. The coefficients a_2 and a_1 are determined by the condition that the function and its first derivative are continuous at the boundary of the knee region. The knee position is defined as the point where the local spectral index of the function above is equal to the mean value of the slopes γ_1 and γ_2 . Some results of the fits are summarized in Table 1.

The positions of the individual knees are plotted in Figure 3. The knee positions are shifted exponentially with increasing atmospheric depth. A fit according to Equation (3) has been applied. The attenuation length determined from these values is $\Lambda_{N_e} = 197 \pm 13 \text{ g/cm}^2$. The quoted error is of statistical kind and follows from the errors of the fit. The resulting attenuation length has to be taken with some precaution. Using other fit functions to determine the knee position yield different results. For example, defining the knee position as the intersection of two straight lines on a logarithmic scale results in an attenuation length of $170 \pm 36 \text{ g/cm}^2$. In Ref. [12], an attenuation length of $222 \pm 28 \text{ g/cm}^2$ for KASCADE data is reported using yet another definition of the knee position. All these results are compatible within their statistical errors, but their relatively large spread indicates the uncertainty resulting from the choice of the function describing the shower size spectra.

Attenuation lengths of other experiments determined by the attenuation of the shower

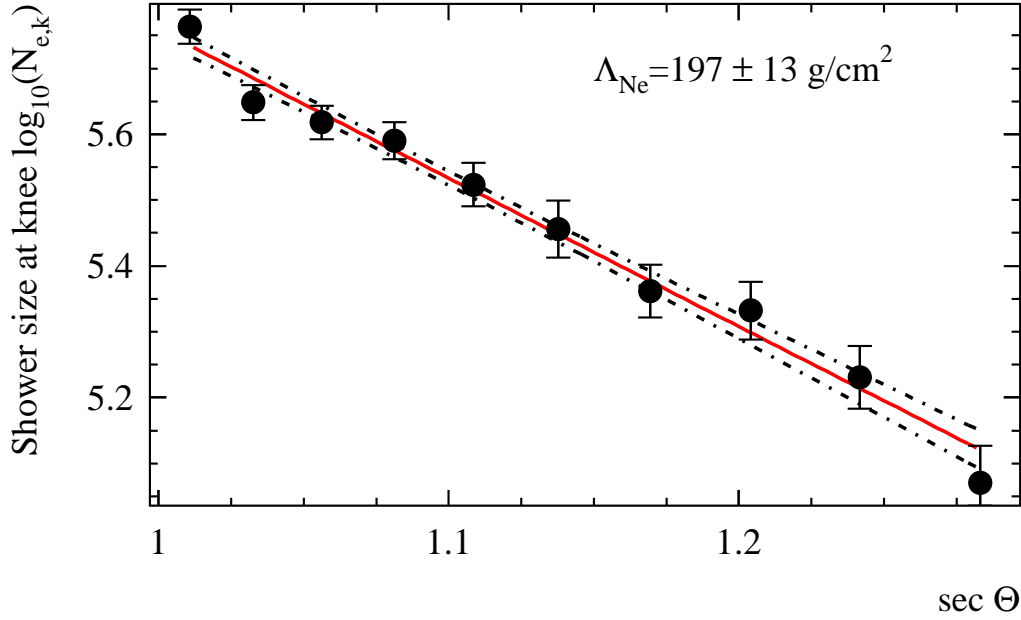


Fig. 3. Knee positions in the differential electron shower size spectra for different angular bins. The lines show an exponential fit and the error region of the fit.

size at the knee are e.g. for EAS-TOP $222 \pm 3 \text{ g/cm}^2$ at an atmospheric depth of 820 g/cm^2 [11] and for MAKET ANI $302 \pm 71 \text{ g/cm}^2$ at 700 g/cm^2 [12]. The tendency of increasing values with decreasing atmospheric depths reflects the change in the longitudinal shower profile while approaching the shower maximum. A comparison of these results with those from KASCADE is therefore not straightforward.

A constant integral flux above the knee would be a verification of the assumptions made in the method of constant intensity. The last column in Table 1 shows the values for the integral fluxes above the knee. A confirmation of the results of the EAS-TOP experiment of a constant flux above the knee within an error of 20% [11] is not possible with the numbers obtained here. Our results match better e.g. with a hypothesis of decreasing flux with increasing zenith angle which could be motivated by the influence of intrinsic shower fluctuations. Again, it must be noticed here that the integral fluxes depend on the method applied to determine the knee positions. The errors of the integral fluxes above the knee quoted in Table 1 are of statistical kind only. The systematic errors due to the choice of the fit function are by far larger. This makes any interpretation concerning a constant flux above the knee very difficult.

3.2 Method of Constant Intensity

To infer the attenuation length by the method of constant intensity the integral electron shower size spectra were grouped into ten bins of zenith angle ranging from

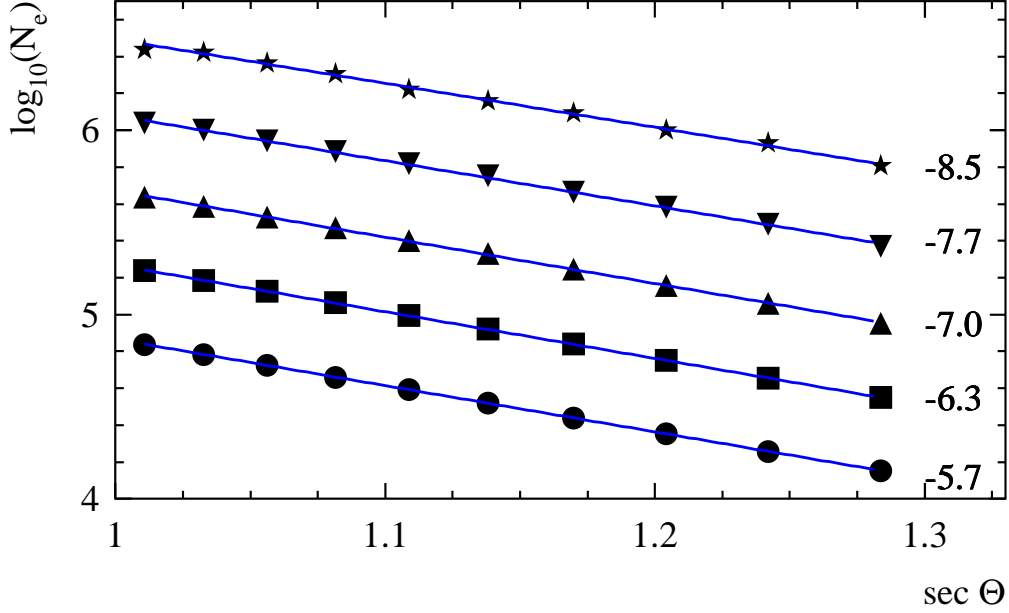


Fig. 4. Electron number as a function of zenith angle for different values of constant intensity. Error bars are smaller than the point sizes. The lines indicate fits using exponential functions, the numbers on the right side are the respective logarithmic fluxes $\log_{10}(j(> N_e))$ in $\text{m}^{-2}\text{s}^{-1}\text{sr}^{-1}$.

0° to 40° . The N_e shifts of the spectra were then analyzed for 18 different values of integral intensities ranging from $6 \cdot 10^{-5}$ to $5 \cdot 10^{-8} \text{ m}^{-2}\text{s}^{-1}\text{sr}^{-1}$. Figure 4 shows the observed attenuation of the shower size with increasing angle for five selected flux values. Again, an exponential behavior is visible. The results of exponential fits to the electron shower sizes at different zenith angles for constant intensities are shown in Figure 5. Each point in this figure corresponds to a certain intensity, which increases from left to right, i.e. the primary energy of the EAS increases from right to left.

From this analysis attenuation lengths between 174 and 190 g/cm^2 are obtained. The result shows an increase of Λ_{N_e} with decreasing flux. This effect is partly due to the correlation between primary energy and atmospheric depth of the shower maximum. Measurements closer to the shower maximum show a flattening of the longitudinal shower profile which is related to increasing values of attenuation lengths. The weak increase of Λ_{N_e} observed towards higher fluxes is in parts due to increasing statistical reconstruction uncertainties for smaller showers. Monte Carlo simulations, described in Chapter 5, confirm this expectation. However, the simulations indicate a stronger effect (5-10 g/cm^2) than observed in the data. This difference is most likely due to the simplified nature of these simulations.

The difference between the attenuation length obtained from the decrease of the shower size at the knee with increasing depth compared to those determined by the method of constant intensities reflects the methodical uncertainties. The more

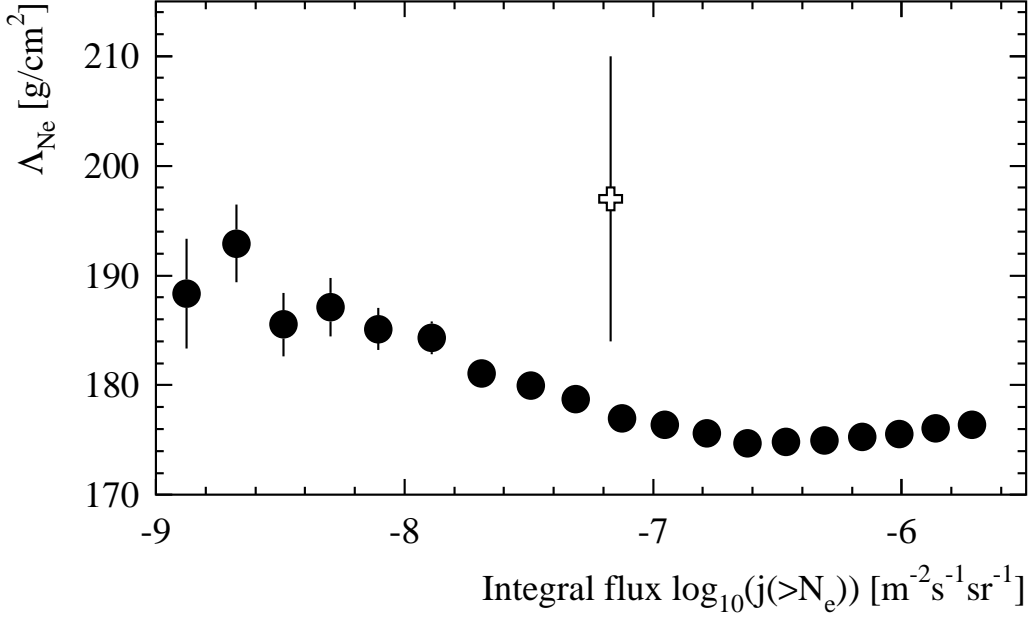


Fig. 5. Attenuation lengths determined by the method of constant intensity (filled points). The attenuation length determined by the knee position is represented by the open symbol, plotted at the weighted mean flux at the knee of $j(> N_{e,k}) = (6.75 \pm 0.13) \cdot 10^{-8} \text{ m}^{-2}\text{s}^{-1}\text{sr}^{-1}$.

or less arbitrary definition of the position of the knee and the strong influence of intrinsic shower fluctuations (see Chapter 5) to both methods are reasons for the observed deviations.

4 Absorption length Λ_{rate}

The absorption length is determined from the integral electron shower size spectra by analyzing the decrease of the shower rate with increasing atmospheric depth for constant N_e . In the following, the atmospheric depth is changed both by the zenith angle of the showers and by using data taken at different atmospheric ground pressures. The main difference between the two methods is the range of variations in slant depth, with the angular method it is up to 300 g/cm^2 and it is about 50 g/cm^2 only with the barometric method. Varying the shower zenith angle in the barometric method, a precise determination of the absorption length can be obtained for different N_e and at different effective atmospheric depths. For example flux variations of showers with $\log_{10}(N_e) > 5.4$ as function of depth are shown in Figure 7.

As mentioned in the introduction, the value of the absorption length is usually related to the attenuation length by multiplication with the local spectral index of the integral electron shower size spectrum. However, this implies the assumption of single component composition and a pure power law spectrum, both of which

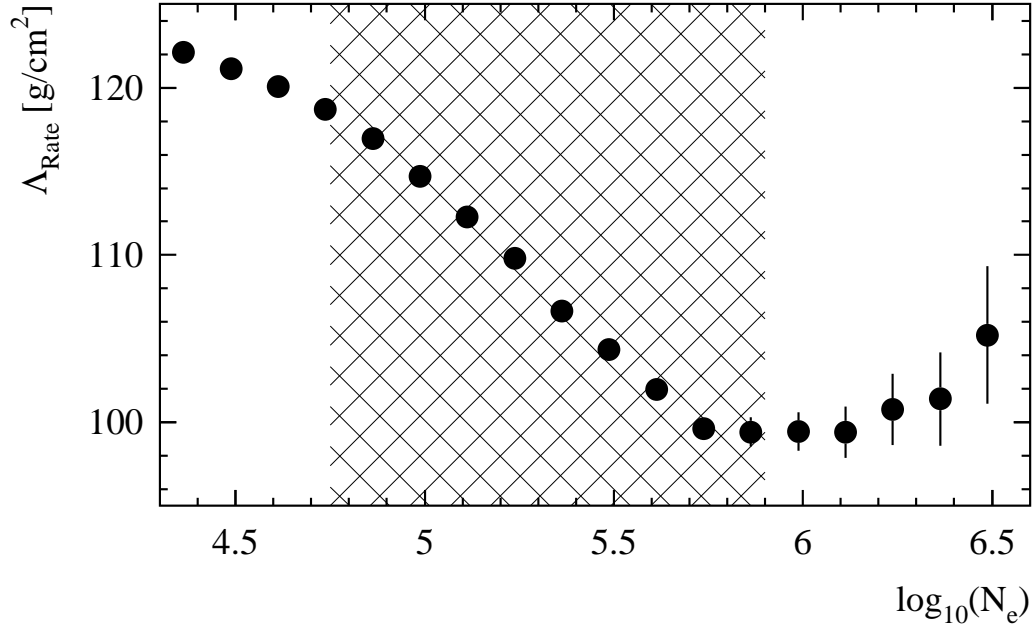


Fig. 6. Absorption lengths versus electron shower size determined by the angular method. The hatched area indicates the region influenced by the changing slopes of the spectra in the knee region.

are not correct. Since the factors in the relation are sensitive especially to the large change in the spectral index in the range of the knee, we refrain from applying this relation to calculate Λ_{rate} from Λ_{N_e} .

4.1 Angular Method

Using the angular method, the absorption length is determined from the integral electron shower size spectra by analyzing the decrease of the flux with zenith angle for given electron shower sizes. An exponential fit of the decreasing flux according to Equation (2) then yields the absorption length. Results are shown in Figure 6 for different thresholds in electron shower size.

The overall trend of decreasing absorption lengths with increasing electron number is caused by the knee in the electron shower size spectra. Scanning from low to high values of N_e over the knee region with its changing slopes at different electron shower sizes in different angular bins mimics a stronger reduction of the fluxes, thereby resulting in a decline of Λ_{rate} . The region where the angular method is not applicable due to this bias is indicated by the hatched area in Figure 6. However, the observed small increase of Λ_{rate} at shower sizes above $10^{6.1}$ electrons, well beyond the knee, exhibits the same behavior as the attenuation lengths in Figure 5 and is related to an effective decrease of the distance between observation level and shower maximum.

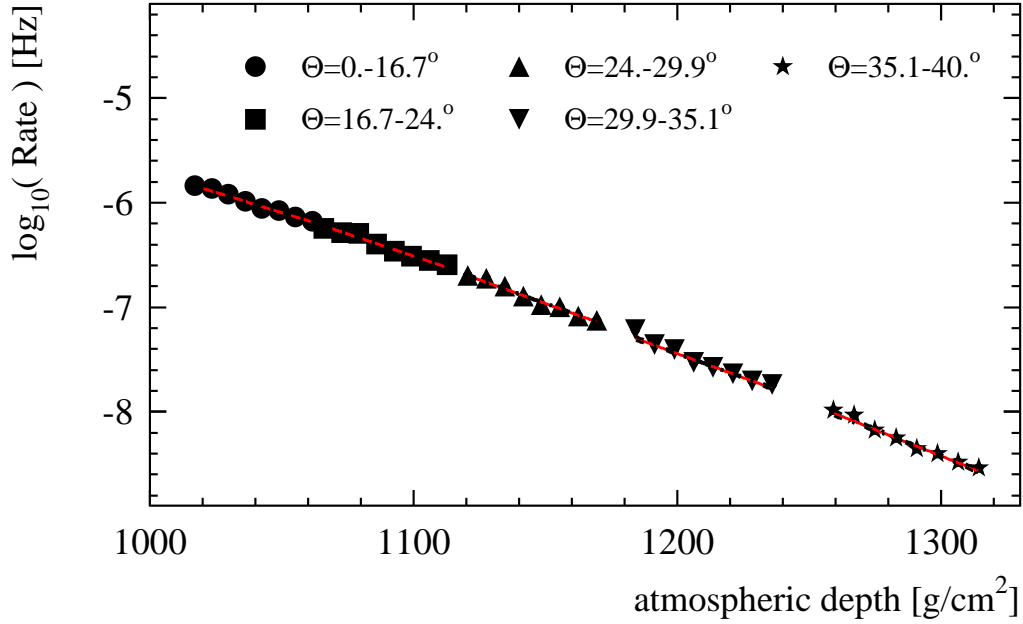


Fig. 7. Variation of showers with atmospheric ground pressure and zenith angle for showers with $\log_{10} N_e > 5.4$. The lines indicate fits with exponential functions.

4.2 Barometric Method

The influence of atmospheric ground pressure is analyzed by counting the number of showers above a certain electron shower size in two hour time intervals. The variation of ground pressure within these time intervals is negligible. A change in the ground pressure of 1 hPa results in a variation of the rate by about 0.7-1% depending on the zenith angle. The mean values of the rate depending on ground pressure and zenith angle, i.e. atmospheric depth are plotted for showers with $\log_{10}(N_e) > 5.4$ in Figure 7. The ground pressure variation is converted to atmospheric depth by

$$X(p(t)) = \frac{X_0}{\cos \Theta} + \frac{p(t) - p_0}{g \cdot \cos \Theta}. \quad (5)$$

$X_0 = 1022 \text{ g/cm}^2$ is the average vertical atmospheric depth at the KASCADE observation level, Θ the mean zenith angle of the angular bin, $p(t)$ the time dependent atmospheric ground pressure, p_0 the mean atmospheric ground pressure and g the gravitational acceleration.

Again, the decrease of intensity is fitted by the exponential law of Equation (2). These fits are performed for six different thresholds in electron shower size and for five different angular bins. Figure 8 shows the absorption lengths obtained by these fits. Both figures, 7 and 8 show a decreasing absorption length with atmospheric depth. This means a deviation of the longitudinal development from the

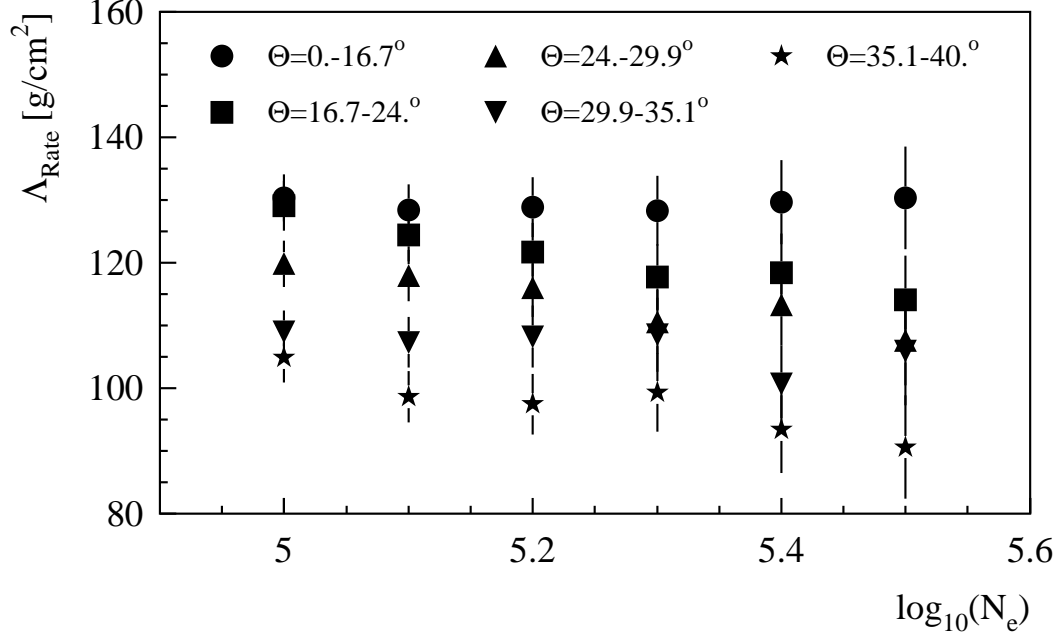


Fig. 8. Absorption lengths determined with the barometric method for showers with different zenith angles.

simple exponential form of Equation (2). Simulated EAS obtained by CORSIKA calculations show a similar behavior.

The absorption lengths determined that way decrease from 130 g/cm² in the first angular bin to 90-100 g/cm² in the last one. The results of the angular and the barometric method are consistent with a decrease of the absorption length by about 10 g/cm² in the observed size region due to the already mentioned change in slope of the spectra.

5 Influence of intrinsic shower fluctuations and reconstruction accuracy on the method of constant intensity

As mentioned before, intrinsic shower fluctuations, reconstruction accuracy of the shower size N_e , and detector response influence the results of most analyses of EAS including the method of constant intensity. To get an estimate of this, a computational analysis using a parameterization of fully simulated EAS is performed.

Electron shower size spectra are simulated with the intrinsic shower fluctuations and the detector response switched on or off. More precisely, the shower size spectra are obtained from a hypothetical primary energy spectrum by

$$\frac{dj}{d \log_{10} N_e} = \sum_{i=p, fe-\infty} \int_{-\infty}^{\infty} \frac{dj_i}{d \log_{10} E} p^i(\log_{10} N_e | \log_{10} E) d \log_{10} E \quad (6)$$

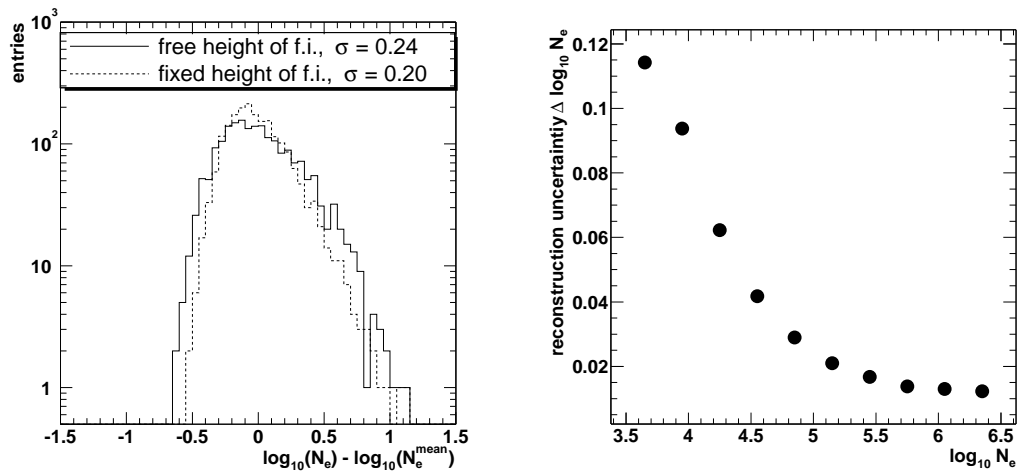


Fig. 9. Left: Intrinsic shower fluctuation for 1 PeV proton showers and 22 degrees zenith angle determined with CORSIKA simulations (solid line). The dashed histogram shows the fluctuations for 1 PeV proton showers with fixed first interaction (f.i.) height of 23.9 km. The distributions are shown relative to their mean value of $\log_{10} N_e \approx 4.6$. Right: reconstruction uncertainty from CORSIKA simulations including detector simulations.

The integral is evaluated by simulation of the primary energy spectra and calculation of the corresponding N_e values, followed by a smearing of the N_e values according to the reconstruction uncertainties and shower fluctuations. The primary energy spectrum is based on an analysis of electron and muon size spectra [13], which exhibits a knee at 4 PeV with spectral indices of -2.7 below and -3.1 above the knee. The composition is represented by a light (proton) and a heavy (iron) component where the protons account for the knee in the total energy spectrum.

The dependency of the electron shower size on the zenith angle is accomplished by using Equation (1) with a constant attenuation length of $\Lambda_{N_e} = 150 \text{ g/cm}^2$. This means that all simulated showers have the same longitudinal development. The different longitudinal profiles in actually measured showers alter the shower size spectra additionally to the effects considered in this chapter but are not taken into account in this analysis.

The kernel function p^i factorizes into three parts, the intrinsic shower fluctuations s^i , the efficiency ϵ^i for the triggering of the measurements, and the reconstruction accuracy r^i of the electron shower size N_e . All three functions are determined with air shower simulations using the CORSIKA [14] package (Version 5.635) with QGSJET [15] as hadronic interaction model and EGS4 [16] for the electromagnetic part of the shower. The subsequent detector simulations are based on the GEANT [17] package and all simulated showers are reconstructed by the same procedure as measured data.

For the fluctuations s^i and the reconstruction accuracy r^i shower size dependent parameterizations of the mean values of Gaussian fit functions to the distributions

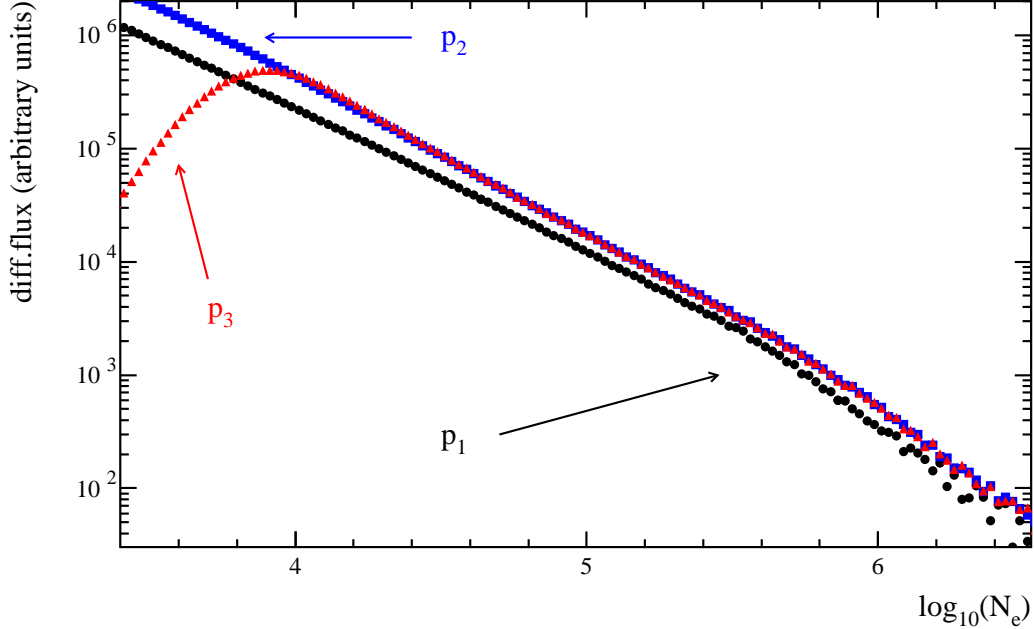


Fig. 10. Monte Carlo shower size spectra with different assumption for the kernel function p^i of Equation (6). p_1 is the spectrum obtained without any fluctuations, p_2 includes intrinsic shower fluctuations and p_3 additionally the reconstruction accuracy as well as the trigger efficiencies.

of the detailed shower simulations are used in the following Monte Carlo calculations. Figure 9 (left) shows as an example one of the distributions used in these parameterizations. The primary particles in the Figure 9 (left) are protons with fixed energies of 1 PeV and 22 degrees zenith angle. Mean and width of this distribution are 4.64 and 0.24 on a logarithmic scale in electron shower size. The right figure shows the statistical uncertainty of the reconstruction versus the electron shower size. As can be seen, the reconstruction error is only important at small electron shower sizes below about $\log_{10}(N_e) < 4.5$.

Three different sets of electron shower size spectra are obtained by calculating the integral in Equation (6) numerically by Monte Carlo methods. The first one (p_1^i), without any fluctuations and detector effects, i.e. $p_1^i = \delta(E - f(N_e))$, the second one (p_2^i) with only shower fluctuations on, and the third one (p_3^i) with the full kernel function as obtained by shower and detector simulations described above. Each set consists of size spectra in the same angular bins as in the data analysis presented in Chapter 3. Figure 10 shows three of these Monte Carlo spectra for all different assumptions on p^i . The intrinsic shower fluctuations shift the spectra to higher values of both electron shower size and intensity and change the slope of the spectra. The reconstruction accuracy has only little influence while the trigger and reconstruction efficiencies becomes more and more important below $\log_{10}(N_e) < 4.5$.

Applying the method of constant intensity to all sets yields the bands of attenuation

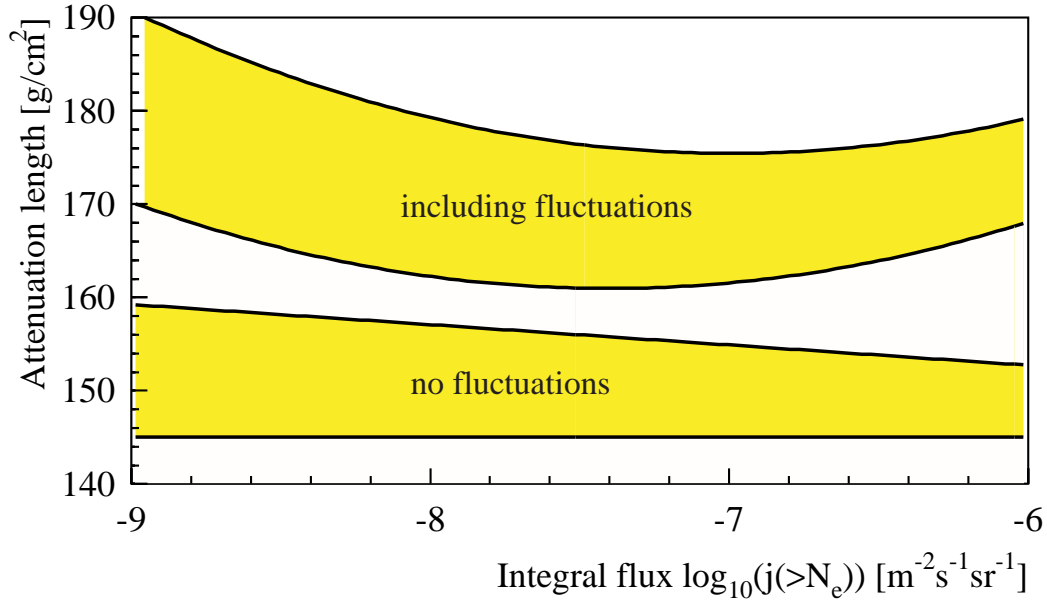


Fig. 11. Attenuation lengths from Monte Carlo spectra determined with the method of constant intensity. The shaded regions reflect the uncertainties due to the choice of the input parameters of the MC. The attenuation lengths in the lower region are determined from average shower size spectra (kernel function p_1^i), the upper ones from taking intrinsic shower fluctuations, statistical reconstruction errors and detector efficiency (kernel function p_3^i) into account.

lengths plotted in Figure 11. For reasons of clarity only the results for p_1^i and p_3^i are plotted. The shaded regions reflect the estimated range of the uncertainty due to the choice of the parameters of the primary energy spectra, composition, and the parameterization of the information from CORSIKA and detector simulations.

The results of Figure 11 demonstrate that fluctuations strongly influence the results of the method of constant intensity; the attenuation lengths are shifted towards higher values by 15-30 g/cm^2 . The attenuation lengths obtained from the mean conversion of the primary energy spectrum to size spectra with kernel function p_1^i reflect the assumed constant $\Lambda_{N_e} \approx 150 \text{ g/cm}^2$ and are in fact quite different from the experimental results shown in Figure 5. On the other hand, the results obtained from simulations taking detector response and intrinsic shower fluctuation into account, i.e. kernel function p_3^i , resemble the data very much. This shows that shower fluctuations have a major influence on the results of the previous analysis in Chapter 3.2. Any interpretation of the attenuation lengths has to take this effect into account. As all the other methods presented in this paper are also sensitive to the form of the shower size spectra, this conclusion applies there as well.

The Monte Carlo study provides also some information about the dependence of the attenuation length on the fluxes. The increase towards higher fluxes is due to the increasing statistical reconstruction uncertainty for smaller shower sizes. In the

low flux region, results are influenced by the changing shape of the spectra due to the knee and due to intrinsic shower fluctuations. The very strong increase of the attenuation length with decreasing fluxes in Figure 5 is not fully reproduced in this solution of Equation (6). One reason for that is the changing slope of the longitudinal shower profile while getting closer to the shower maximum, i.e. here with increasing electron shower size. This effect is not included in the simulations. Another reason could be the simplified parameterization of the fluctuations by Gaussian functions in $\log_{10} N_e$. Simulations show especially for the proton component asymmetric distributions with very long tails towards larger electron shower sizes (see Figure 9). Also the assumption of a two component composition instead of a more realistic one is a strong simplification and influences these results. However, the presented sensitivity of the method of constant intensity to shower fluctuations and the trend of observing attenuation lengths with a bias towards larger values are not affected by these simplifications.

6 Remarks about absorption lengths and p-air inelastic cross sections

The term absorption length is often used in literature in connection with p-air inelastic cross sections. This absorption length, in the following called Λ_{cross} , describes something different than the one used in this paper.

The idea of the cross section analysis, the so-called constant N_e-N_μ method is based on the assumption that EAS with about the same N_e and N_μ at ground level have developed through the same slant depth [3]. Analyzing the zenith angle dependence of the flux of these shower samples determines then Λ_{cross} . The samples are enriched of proton initiated showers by selecting showers with the largest number of electrons. The proton-air cross section is then calculated by the formula $\Lambda_{cross} = k \cdot 14.5 \cdot m_p / \sigma_{p-Air}^{inel}$. The simple factor k is used to correct for the influence of shower fluctuation and detector response [3,18,19]. It includes properties of the underlying hadronic interaction model.

A good correlation of the position of the first interaction point to the electron shower size at observation level is required for the N_e-N_μ method. For example Figure 9 shows the N_e distribution of 1 PeV proton showers. The dotted line is the result of simulations using a fixed depth of the first interaction. In case of no intrinsic shower fluctuations (i.e. perfect correlation between depth of first interaction and observed electron shower size) this dotted curve would be a narrow peak at $\langle \log_{10} N_e \rangle \approx 4.6$. The comparison with the result of the full simulations shows that intrinsic shower fluctuations dominate over fluctuations due to the first interaction point. Similar conclusions, but for higher energies, were reached in an independent study in [20]. This means that a shower with large observed N_e is not necessarily a shower starting deep in the atmosphere (see Fig.7 in [20]). Therefore, it appears

doubtful whether the constant N_e - N_μ method could give reliable results concerning the proton air-cross section for primary energies relevant for KASCADE.

7 Summary

We have presented a comprehensive measurement of the atmospheric attenuation of the electromagnetic component in EAS. The data are based on the detector array of the KASCADE experiment. Both the attenuation and absorption length have been reconstructed for shower sizes in the interval $\log_{10} N_e = 4.5$ to $\log_{10} N_e = 6.5$ covering the energy range of the knee. The most important experimental findings can be summarized as:

- The attenuation length increases with electron numbers $N_e > 10^{5.5}$ from $\Lambda_{N_e} = 175 \text{ g/cm}^2$ to 194 g/cm^2 .
- The angular method for the determination of the absorption length appears almost inapplicable in the knee region due to the changing slopes in the size spectra. Well above the knee values between 100 and 110 g/cm^2 were obtained.
- The longitudinal development deviates from a simple exponential assumption and steepens with increasing atmospheric depth.
- Intrinsic shower fluctuations cause an increase of the attenuation lengths by about 15 - 30 g/cm^2 . This shift depends on the shower size and cannot be neglected.

Furthermore, the experimental studies emphasize the need to account for methodical effects as well as for shower and sampling fluctuations when attempting quantitative interpretations of the attenuation and absorption lengths. It is hoped that the detailed analyses of experimental and simulated data presented here will help to improve the understanding of the experimental input to calculations, thereby reducing systematic differences between different approaches.

Acknowledgments

The authors are indebted to the members of the engineering and technical staff of the KASCADE collaboration who contributed with enthusiasm and engagement to the success of the experiment. The work has been supported by the Ministry for Research and Education of the Federal Government of Germany. The collaborating institute in Lodz is supported by the Polish State Committee for Scientific Research (grant No. 5 P03B 133 20) and the Institute of Bucharest by a grant of the Romanian National Academy for Science, Research and Technology. The KASCADE work is embedded in the frame of scientific-technical cooperation (WTZ) projects between Germany and Romania, Poland, and Armenia.

References

- [1] S. Yoshida et al., *Astropart. Phys.* **3** (1995) 105.
- [2] M. Ave et al., astro-ph/0112253, *Astropart. Phys.* in print
- [3] T. Hara et al., *Phys. Rev. Lett.* **50** (1983) 2058.
- [4] P. Doll et al., Report KfK 4686, Kernforschungszentrum, Karlsruhe, 1990.
- [5] T. Antoni et al., (KASCADE Collaboration), submitted to *Nucl. Instr. Meth.* (2003).
- [6] K. Kamata, J. Nishimura, *Prog. Theoret. Phys. Suppl.* **6** (1958) 93.
- [7] K. Greisen, *Progress in Cosmic Ray Physics* **3**, North Holland Publ. 1965.
- [8] T. Antoni et al., (KASCADE Collaboration), *Astropart. Phys.* **14** (2001) 245.
- [9] M. Nagano et al., *J. Phys. G: Nucl. Phys.* **10** (1984) 1295.
- [10] R. Glasstetter et al., (KASCADE Collaboration), *Proc. 25th ICRC, Durban*, **2** (1997) 157.
- [11] M. Aglietta et al., (EAS-TOP Collaboration), *Astropart. Phys.* **10** (1999) 1.
- [12] A.A. Chilingarian et al., *Proc. of the Workshop ANI 99, Report FZKA 6472, Forschungszentrum Karlsruhe, 1999*, 43.
- [13] R. Glasstetter et al., (KASCADE Collaboration), *Proc. 26th ICRC (Salt Lake City)*, **2** (1999) 222.
- [14] D. Heck et al., Report FZKA 6019, Forschungszentrum Karlsruhe, 1998.
- [15] N.N. Kalmykov, S.S. Ostapchenko, A.I. Pavlov, *Nucl. Phys. B. (Proc. Suppl.)* **52B** (1997) 17.
- [16] W.R. Nelson, H. Hirayama, and D.W.O. Rogers, Report SLAC 265 (1985), Stanford Linear Accelerator Centre.
- [17] Application Software Group, *GEANT - Detector Description and Simulation Tool*, CERN, Geneva, 1993.
- [18] M. Honda et al., *Phys. Rev. Lett.* **70** (1993) 525.
- [19] M. Aglietta et al., (EAS-TOP Collaboration), *Nucl Phys. B (Proc. Suppl.)* **75A** (1999) 222.
- [20] J. Alvarez-Muñiz et al., *Phys.Rev.D* **66** (2002) 123004.